PAPER • OPEN ACCESS

Reshapeable, rehealable and recyclable sensor fabricated by direct ink writing of conductive composites based on covalent adaptable network polymers

Reshapeable, rehealable and recyclable sensor fabricated by direct ink writing of conductive composites based on covalent adaptable network polymers

Xu He[1], **Yuchen Lin**[1], **Yuchen Ding**[1], **Arif M Abdullah**[1], **Zepeng Lei**[2], **Yubo Han**[3], **Xiaojuan Shi**[1,4], **Wei Zhang**[2] **and Kai Yu**[1,*] ![ORCID]

[1] Department of Mechanical Engineering, University of Colorado Denver, Denver, CO 80217, United States of America
[2] Department of Chemistry, University of Colorado Boulder, Boulder, CO 80309, United States of America
[3] School of Electronic and Information Engineering, Beijing Jiaotong University, Beijing 100044, People's Republic of China
[4] National Key Laboratory of Science and Technology on Advanced Composites in Special Environments, Harbin Institute of Technology, Harbin 150080, People's Republic of China

E-mail: kai.2.yu@ucdenver.edu

Abstract

Covalent adaptable network (CAN) polymers doped with conductive nanoparticles are an ideal candidate to create reshapeable, rehealable, and fully recyclable electronics. On the other hand, 3D printing as a deterministic manufacturing method has a significant potential to fabricate electronics with low cost and high design freedom. In this paper, we incorporate a conductive composite consisting of polyimine CAN and multi-wall carbon nanotubes into direct-ink-writing 3D printing to create polymeric sensors with outstanding reshaping, repairing, and recycling capabilities. The developed printable ink exhibits good printability, conductivity, and recyclability. The conductivity of printed polyimine composites is investigated at different temperatures and deformation strain levels. Their shape-reforming and Joule heating-induced interfacial welding effects are demonstrated and characterized. Finally, a temperature sensor is 3D printed with defined patterns of conductive pathways, which can be easily mounted onto 3D surfaces, repaired after damage, and recycled using solvents. The sensing capability of printed sensors is maintained after the repairing and recycling. Overall, the 3D printed reshapeable, rehealable, and recyclable sensors possess complex geometry and extend service life, which assist in the development of polymer-based electronics toward broad and sustainable applications.

Keywords: bond exchange reactions, polyimine, covalent adaptable networks, direct ink writing, rehealable electronics, recyclability

---

* Author to whom any correspondence should be addressed.

1. Introduction

Polymer-based electronics and sensors have vast potential for future microsystems applications. They possess many advantages over conventional inorganic semiconductor-based systems, including the low cost, lightweight, flexibility, and the ability to integrate a wide variety of functions on a single platform. When using crosslinking thermosets as matrix materials, the electronics further exhibit enhanced stability at high temperatures, resistance to chemical corrosion, and the ability to bear external loading, which are appealing features for high-performance electronics applications. However, the use of thermosets leads to ever-increasing electronic wastes due to their unrepairable and unrecyclable nature [1]. It was reported that 50 million tons of electronic waste is generated each year, and 70% of that waste goes directly to landfills [2, 3]. Therefore, the development of easily recyclable and reprocessible polymeric electronics could significantly reduce the production cost and hazard to our environment, thus enabling their sustainable development.

Within the past ten years or so, a revolutionary group of new polymers, called covalent adaptable network (CAN) polymers [4–12], have been developed, which can reorganize microscale network configurations (e.g. via bond exchange reactions, BERs) when an environmental stimulus is given (e.g. heat, light, moisture), leading to the shape-reforming and self-healing capabilities of the materials [9, 13–20]. In addition, CANs are shown to be fully depolymerized in a suitable organic solvent and re-polymerized into near-identical networks when heated, which enables the primary recycling of thermosetting polymers [21–29] and their composites [30–32]. Recent studies employed CANs as the matrix material to create conductive polymer composites for the applications of rehealable electrical conductors [33, 34], sensors [35–38], or batteries [39]. William *et al* [34] developed a self-healing conductor with conductivity $\sim 10^{-3}$ S cm^{-1}. The system was crosslinked between *N*-heterocyclic carbenes and transition metals, which were both electrically conductive and structurally dynamic. Damaged areas could be healed at 150 °C in the presence of dimethylsulphoxide vapor. Compared to self-healing polymers loaded with microcapsules containing healing agents [40–43], the application of CAN composites allows for repeatable healing of the same damaged area while maintaining sufficient conductivity. For example, supramolecular hydrogels with dynamic hydrogen bonds were used to fabricate conductive composites with Nickel micro-particles [36]. After being damaged, the material was healed in 15 s at room temperature. The damage-healing cycle was repeated at the same location three times, and the material maintained at least 90% of its original conductivity in each cycle.

Conductive CAN composites show great potential to create the next generation green and sustainable electronics with promoted reliability, extended service life, and application areas. However, their detailed sensing capability (e.g. temperature-dependent conductivity) and the application potentials for reprocessible and recyclable electronics are inadequately investigated. On the other hand, the sustainable development of polymer-based electronics requires an efficient and economical manufacturing method. Conventional methods, such as surface coating, deposition, and transfer printing, require complicated processes and are time-consuming. Mass production is required to settle the overhead cost of tools and labor for assembly. More importantly, they are incapable of achieving a highly non-regular but precisely controlled material distribution within a single composite. In great contrast, 3D printing allows for the precise placement of multiple materials at micro- or nano-scale resolution with low cost and essentially no restrictions on the geometric complexity of the spatial arrangement. Due to the low cost-per-part and high design freedom, 3D printing is ideal for rapid prototyping and product development [44–46].

The potential of 3D printing as a deterministic manufacturing method for polymer-based electronics motivates us to incorporate conductive CAN composites into the printing process to fabricate rehealable and recyclable electronics. Various methods that enable the conductivity of polymers have been studied. The most common one method incorporates conductive nanoparticles, such as carbon nanotubes and carbon black, to form conductive pathways within the composites. Recently, liquid metal has attracted widespread interest to fabricate flexible and stretchable electronics. Significant progress has been made to promote its application potential. For example, He *et al* [47, 48] developed material and processing techniques to promote the wettability of liquid metal and enable its self-sintering property, which dramatically enhanced its compatibility with various advanced manufacturing processes. On the other hand, conductive organic polymers with specially designed chemical compositions have been developed to offer high electrical conductivity for electronic applications [49–51]. They might be able to exhibit interfacial welding and recycling capabilities by incorporating appropriate dynamic covalent bonds on the chain backbone. In this work, we chose multi-walled carbon nanotubes (MWCNTs) as conductive additives for CAN composites [52–59]. The manufacturing process is more accessible to researchers without strong chemistry or physics backgrounds. The idea of using BERs to enable the shape-reforming, repairing, and recycling of conductive composites might be extended to other advanced polymer and composite systems.

The recently developed polyimine CAN is used as the model material, which is a representative CAN system. It requires low temperatures for material reprocessing and does not require a catalyst to trigger the internal BERs. Direct-ink-writing (DIW) 3D printing is adopted, which has been a popular approach to print thermally-curable thermosets [60–62] and various electronics, such as small antennas [63], batteries [64–68], light-emitting diodes [69, 70], and soft sensors [71]. To prepare the DIW printable ink, the polyimine is first depolymerized in an amine-containing solvent and mixed with different contents of MWCNTs. After printing, the printouts are moved into an oven to evaporate the solvent and cure the network. The approach can be extended to other types of conductive CANs by using a suitable reactive solvent. The printed polyimine sensors are shown to exhibit excellent sensing, shape-reforming, self-healing, and recycling capabilities.

2. Results and discussions

2.1. Ink preparation for the DIW printing of conductive polyimine composites

The overall ink preparation process for the DIW printing of conductive CANs is shown in figure 1. The polyimine CAN was initially synthesized using the terephthaldehyde (dialdehyde) and diethylenetriamine (diamine) as the monomers, and the tris (2-aminoethyl) amine as the cross-linker (figure 1(a)), which were purchased from Sigma Aldrich (St. Louis, MO, USA) and used in their as-received condition. The detailed synthesis procedure can be found in the study by Taynton *et al* [9]. The synthesized polyimine was in the glass state at room temperature with a glass transition temperature (T_g) around $\sim$50 °C. The network contains dynamic C$=$N bonds on the chain backbone (highlighted in figure 1(a)), which enables the imine exchange reactions when the temperature exceeds $\sim$60 °C. The dynamic network exhibited three unconventional features (figure 1(b)): first, when the network deformed, the internal stress can be effectively released during the chain cleavage of a BER, leading to permanent shape-reforming (or reprocessing); second, when the polyimine pieces come into contact, macromolecular chains connect on the interface due to BERs, enabling the interfacial welding and repairing capability; third, the network can be fully depolymerized using an amine-containing solvent and fully recycled with near-identical thermomechanical properties.

Propylamine (Sigma Aldrich) was used for the network depolymerization, wherein the polyimine scraps were immersed in the propylamine solvent at 80 °C. The weight ratio between the solvent and polymer was set to be 1:2. The solvent molecules diffused into the network and participated in BERs with the dynamic bonds, which led to the chain cleavage from the backbone. After being heated for 30 min, the polyimine CAN was fully depolymerized into soluble segments (figure 1(c)).

The MWCNTs purchased from Sigma Aldrich were added into the depolymerized polymer solution (figure 1(d)). The average length of the MWCNTs was $\sim$1 μm, and their diameter was $\sim$50 nm. Different amounts of MWCNTs (5 wt%, 10 wt%, 15 wt%, 17 wt%, 20 wt%, 22 wt%, and 25 wt% compared to the polymer weight, respectively) were added. About 10 wt% nano-clay platelets (Nanomer® I.28E clay, Sigma Aldrich) were added at this stage to introduce the shear-thinning effect to the printable ink. The liquid mixture was then transferred to a high-energy sonicator (SONICS-44349N) for 12 h to improve the separation of MWCNTs. The output amplitude was 60%. Note that the solvent mixture at this stage was diluted with low viscosity. For the DIW printing, the printable ink should exhibit a relatively high modulus and yielding stress so it can retain the filamentary form after extrusion. To this end, the ink was heated at 80 °C in an open environment to be partially cured, wherein the depolymerized chain segments re-connected at end groups, and the released solvent molecules evaporated out of the system, leading to the increment of resin viscosity and yielding strength. Printing the partially cured

resin also minimizes the volume shrinkage of the polyimine composites during the post-curing step.

The viscosity and storage modulus of the prepared inks with different MWCNT loadings after being heated for 30 min are shown in figure 2. As shown in figure 2(a), when the resin was mixed with nano-clay and MWCNTs, its apparent viscosity dramatically increased, and the ink exhibited notable shear thinning effect. With 10 wt% nano-clay, the ink viscosity at 1×10^{-3} s^{-1} was $\sim$2 $\times 10^3$ Pa s, which is three orders of magnitude higher than that of the pure resin. The ink viscosity further increased to $\sim$10^5 Pa s with 25 wt% MWCNTs added. But due to the shear-thinning effect, the ink exhibits an apparent viscosity of $\sim$3 kPa s at $\sim$200 s^{-1}.

As shown in figure 2(b), the shear modulus of the polyimine resin without additives was $\sim$1.45 Pa, which was independent of shear stress. The shear modulus increased dramatically with the content of nano-clay and MWCNTs in the ink. With 10 wt% nano-clay and 25 wt% MWCNTs, the initial ink modulus at the low-stress level increased to $\sim$10^6 Pa. The shear yielding stress is defined as the stress level when the modulus starts to decrease significantly. It was $\sim$700 Pa. The polyimine conductive composite inks with 10 wt% nano-clay and 25 wt% MWCNT were used for the DIW 3D printing. Note that due to the considerable amount of MWCNTs in the ink, its viscosity was much higher than the ink without MWCNTs. A deposition nozzle with a relatively big diameter (1.63 mm) was used for the printing to promote extrusion.

2.2. Mechanical performance and conductivity of the printed polyimine composites

After printing, the polyimine and its conductive composites were subject to post-curing to evaporate the solvent and fully polymerize the network (see the Experimental Section for detail). 3D printed polymeric components usually exhibit weak interfaces due to the non-covalent bonding. For the DIW printed thermally-curable thermosets and their composites, the material remains in a viscous oligomer state after filament extrusion. During the post-curing step, interfacial polymerization created interfaces among filaments being connected with covalent bonds, leading to isotropic mechanical and electrical properties. Therefore, the performance of the printed polyimine composites is not dramatically limited by the printing directions. This feature is desirable for the design and advanced manufacturing of polymeric electronics as it assists to release the manufacturing constraints during 3D printing.

A printed single-layer polyimine conductive composite is shown in figure 3(a), wherein the printing direction of the filaments is vertical. Then, the composite was cut in different directions about the printing direction (0°, 45°, and 90°). The obtained samples were tested using the uniaxial tension tests at room temperature. Figure 3(b) shows their stress–strain relationship. It is observed that the printed composites exhibit close mechanical properties in different printing directions, which suggests robust interfaces among filaments connected by covalent bonding. Previous studies on fused deposition modeling indicate that the polymer chains might
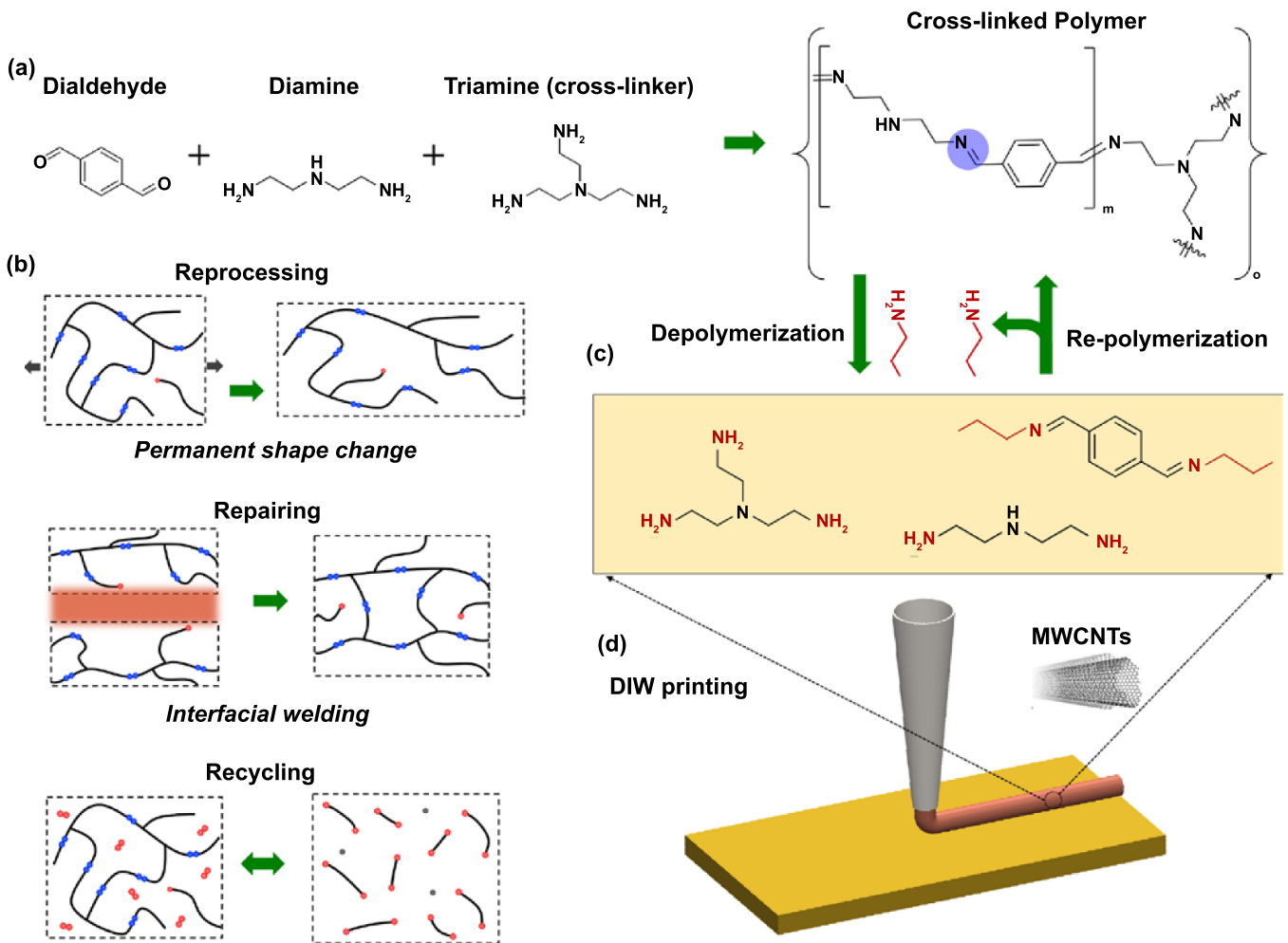
Figure 1. (a) Polyimine synthesis using the dialdehyde and diamine as the monomer, and triamine as the cross-linker. The blue circle in the cross-linked network highlights a dynamic $C=N$ bond on the chain backbone. (b) Schematic views showing the mechanisms of reprocessing, repairing, and recycling of the polyimine networks. (c) The synthesized polyimine CANs can be fully depolymerized and recycled using propylamine solvent. (d) The depolymerized polymer solution was partially cured and mixed with MWCNTs as the printable ink.
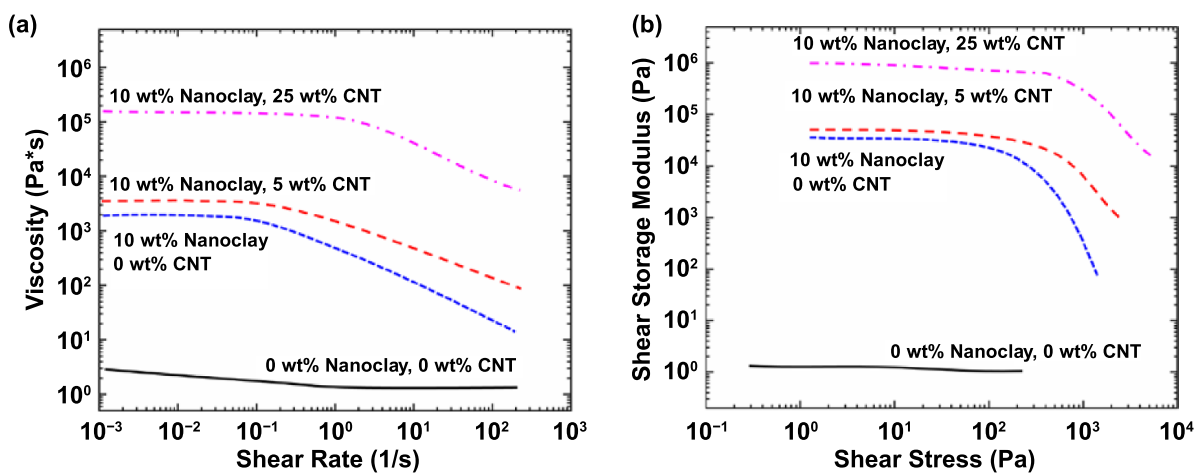
Figure 2. Viscosity and shear modulus of the inks with different MWCNT contents. (a) Apparent viscosity at different levels of shear rate. (b) Shear storage modulus at different levels of shear stress.
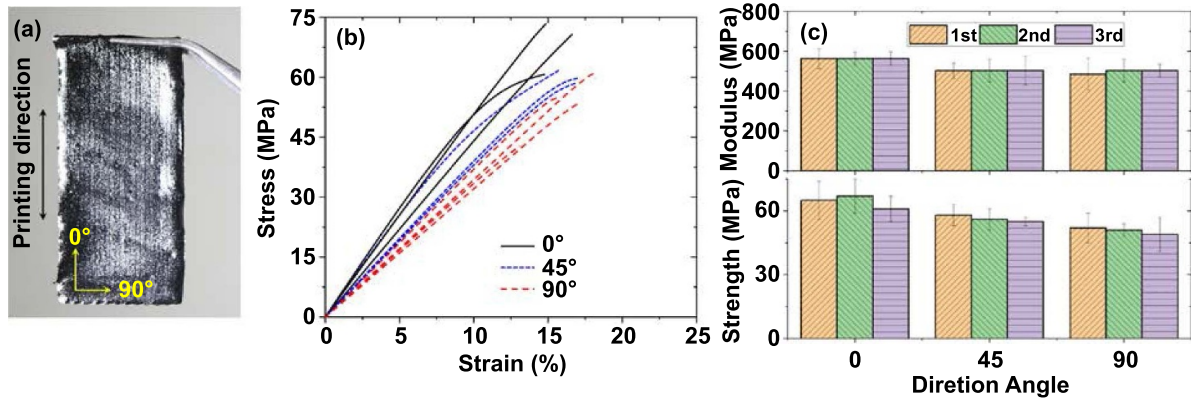
Figure 3. Mechanical properties of the printed conductive polyimine. (a) Appearance of a printed single-layer polyimine composite. (b) The stress–strain relationship of the printed composites at room temperature in different printing directions. (c) The elastic modulus and strength of printed composites during the recyclable 3D printing.

be aligned due to the shear force during filament extrusion [72–75]. However, for the polyimine composite filaments created by DIW, an isotropic arrangement of chain segments is anticipated because the crosslinking and random BERs during post-curing continuously disturb any chain alignments.

The printed polyimine composites were then depolymerized in the propylamine solvent, partially cured, and loaded into the DIW printer for the next printing cycle. No supplementary material was added during this process. The printing was repeated two times and the mechanical properties of the printed composites in each cycle are compared in figure 3(c). It is seen that both the elastic modulus (within the first 5% stretch) and ultimate strength maintain the same level. The modulus and strength are 490 MPa–520 MPa, and 54 MPa–62 MPa among these printing cycles. The developed polyimine composites show excellent repeatability for recyclable 3D printing.

The conductivities of the printed polyimine composites with different MWCNT loadings were determined using the four-point probe resistivity measurements at room temperature. As shown in figure 4(a), a DIW printed thin film sample (1.6 mm thinness) was passed through a direct current, I, through two outer probes (24 mm in distance). The voltage between the two inner probes (16 mm in distance), U, was used to determine the resistivity, $\rho = \pi / ln2 \times U/I$, wherein the coefficient accounts for the measurements over thin-film samples with current rings developed. The conductivity of polyimine composite is $\sigma = 1/\rho$.

The conductivities of printed polyimine composites with different MWCNTs loadings are shown in figure 4(b). They were measured in both longitudinal and transverse directions with respect to the printing pathway. It is observed that the conductivity increases with the amount of MWCNT because more conductive pathways are formed within the composites. It also shows that the conductivity is similar in both longitudinal and transverse directions. For example, with 25 wt% MWCNTs, the longitudinal conductivity and transverse conductivity are 1.5 s cm^{-1} and 2.4 s cm^{-1}, respectively. During the post-curing of the polyimine composites, in addition to the

diffusion and interfacial welding of polymer chains, the conductive MWCNTs may diffuse around the interface to form conductive pathways. Thus, the printed composites exhibit less significant directional dependence of their conductivity.

As shown in the inset figure of figure 4(b), the relationship between the measured conductivity and the content of MWCNT can be captured using a Gaussian function:

$$\sigma = a \exp\left[-\frac{(\varphi - b)^2}{2c^2} \right], \tag{1}$$

where $a = 2.62$ s cm^{-1}, $b = 0.046$, and $c = 0.27$. From the curve, it is estimated that the critical MWCNT content for notable conductivity increment is ∼15 wt%. Note that there are existing studies on conductive composites showing that an equivalent conductivity can be realized using less MWCNT loading [76]. Due to Van der Waals forces, individual MWCNTs tend to attract each other. To improve the composite conductivity, a key procedure is to separate MWCNT aggregates (e.g. using ultrasonic dispersion) to enable a uniform distribution of nanoparticles. However, the separation of MWCNTs is challenging when it comes to the DIW printing of thermally curable composites. The viscous resin experiences extended processing times, typically a few hours to a day, before the network is fully polymerized. Due to the poor compatibility between MWCNT and the viscous resin in thermodynamics, the nanoparticles may aggregate again to form notable clusters during the ink pre-curing and subsequent material post-curing at high temperatures. This will occur even if a uniform dispersion of MWCNTs is realized during the initial resin mixing. This also explains why the relationship between the measured conductivity and MWCNT content does not follow the classic power-law network percolation theory [77]. In this paper, all of the polyimine composites were printed and cured using the processing conditions mentioned in the experimental section. Future studies should address how to improve the conductivity of 3D printing polyimine composites using fewer MWCNTs.
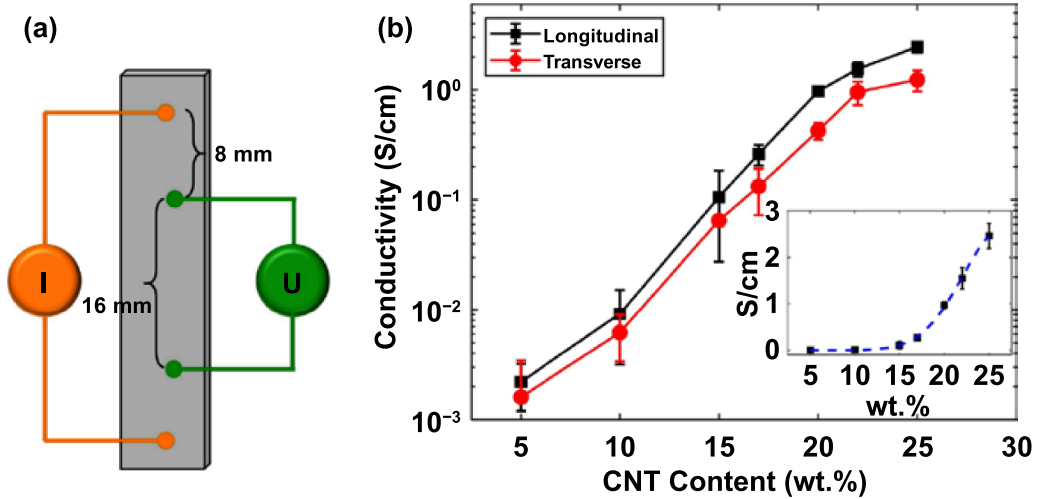
Figure 4. (a) Schematic view of four-point probe resistivity measurements. (b) The conductivity of the printed polyimine composites with different MWCNT loading in both longitudinal and transverse directions of the filament. Inset figure: the relationship between the measured longitudinal conductivity and the MWCNT content is captured using a Gaussian function.

Existing studies on the conductive CAN sensors focus on improving the conductivity at room temperature [33–36]. There are few studies that reveal how the conductivity evolves with temperature, which is an important aspect for sensor and electronics applications. Herein, the temperature-dependent conductivity of the polyimine composites with 20 wt%, 22 wt%, and 25 wt% MWCNTs was tested, and the results are shown in figure 5(a). During the tests, the temperature increased from 25 °C to 150 °C at 2.0 °C min^{-1}. It was observed that all the specimens with different MWCNT contents have a similar resistance trend. The conductivity first decreases with temperature, showing a positive temperature coefficient (PTC) of conductive materials. After passing a specific temperature, the conductivity tends to increase linearly with temperature, showing a typical negative temperature coefficient (NTC).

The interesting conductive behavior of CAN composites can be explained below. As illustrated in the inset picture of figure 5(a), when the temperature increases from room temperature, the internal BERs of polyimine gradually activate, which leads to active chain cleavage and reconnection within the network, accompanied by dramatic thermal expansion of the material. As revealed in our recent study [78], when the temperature of an epoxy CAN approaches the BER activation temperature, the thermal expansion coefficient is ∼2–4 times higher than that in the rubbery state. This active chain movement and thermal expansion increase the distance between conductive MWCNTs and disrupt the conductive network formed in the material as the direct contact of MWCNTs is destroyed and further evolves into wide gaps. Therefore, the conductivity of polyimine composites initially decreases with the temperature. The conductivity decrease reaches a maximum when the original conductive pathways are fully reorganized. The polyimine composites then start to show the conventional NTC effect, where temperature promotes electron movement, and the material conductivity increases with the temperature. It is also seen that the conductivity of a

polyimine composite with lower MWCNT content continues decreasing until a higher temperature is reached. This might be because a lower MWCNT content leads to a lower density of conductive pathways. In this context, more intense BERs at higher temperatures are required to re-organize the conductive pathways.

Overall, the results in figure 5(a) reveal the sensing capability of conductive polyimine composites. The co-existence of PTC and NTC effects enable the self-regulating functions of conductive CAN composites and expand their potential applications in the fields of automobiles, spacecrafts, smart buildings, and medical equipment. For example, they can be used as self-controlled heaters with constant input voltage. When a specific temperature is reached, it will stabilize because the material resistance starts to increase if the temperature goes higher, leading to a lower power of Joule heating.

The conductivity of the 3D printed specimen was measured at room temperature with different tensile and compressive strains. Figure 5(b) shows the conductivity of polyimine composites as a function of tensile strain. It was observed that the conductivity decreased for all specimens with different MWCNTs contents. This is because that the average distance (or tunnel gap) among the conductive MWCNTs increases with the tensile strain. Conversely, the conductivity increased as a function of compressive strain due to the decreased MWCNT distance (figure 5(c)). The changes in conductivity as a function of strain are shown to follow a linear relationship, which can be described using the following simple function:

$$\sigma = \sigma_{\varepsilon=0}(1 - \alpha\varepsilon), \qquad (2)$$

where $\sigma_{\varepsilon=0}$ is the initial conductivity without deformation. $\alpha = 3$ and 1.5 for the tension and compression, respectively. The different fitting parameters might result from the different deformation or boundary conditions being applied during the measurement. It suggests that the conductive polyimine
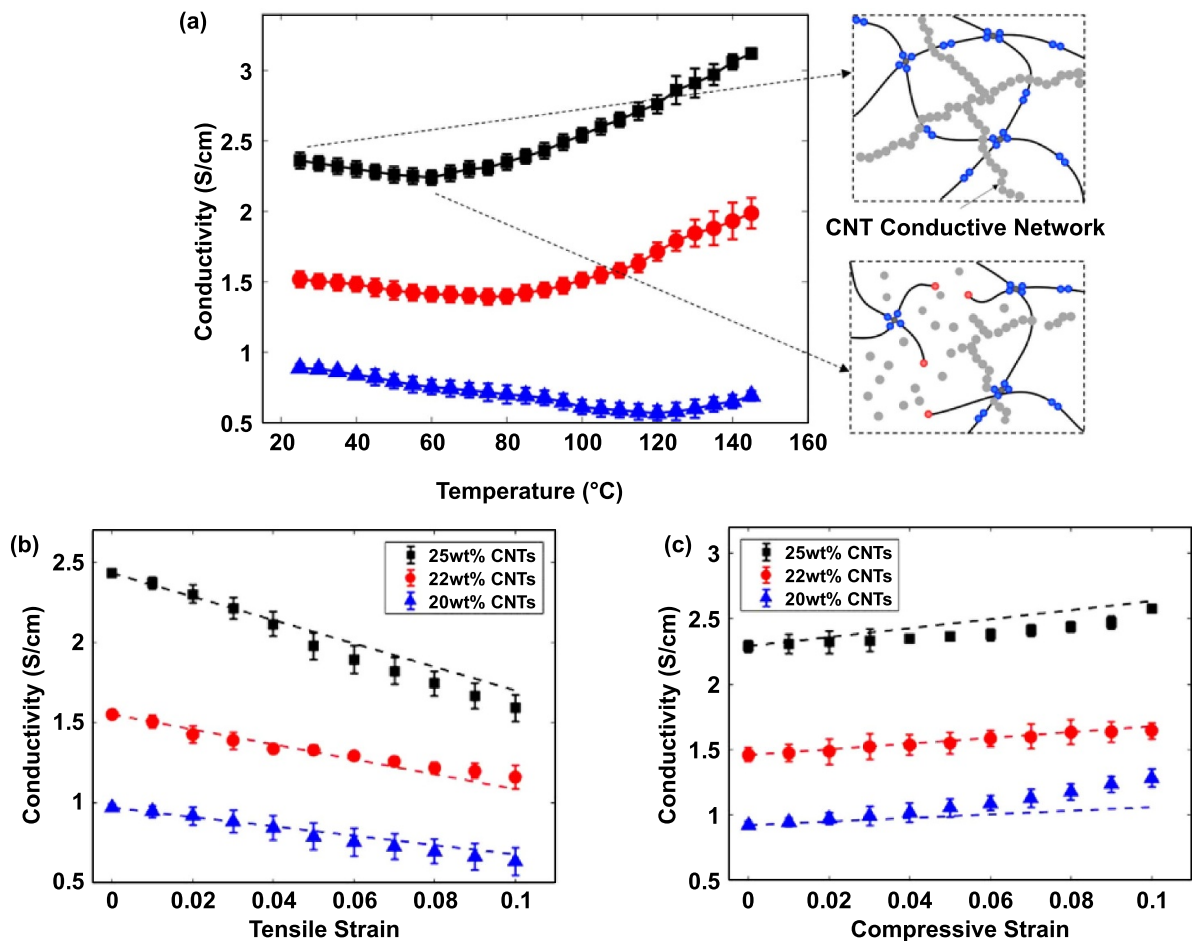
Figure 5. Sensing ability of the printed polyimine composites as a function of (a) temperature, (b) tensile strain, and (c) compressive strain.

is more sensitive to the tensile strain. The linear relationship indicates that the polyimine composites have the potential to be used as the strain sensor.

2.3. Shape-reforming ability of the printed polyimine composites

The conductive polyimine composites exhibit shape-reforming capability due to the malleability of the polymer matrix. This could extend their applications as flexible electronics as it can be readily mounted on the component surfaces for sensing or performing other functions. The previous studies show after a CAN sample releasing the internal stress, it can permanently fix the new configuration [6, 16, 31, 79]. However, the reshaping capability of the CAN composites with considerable MWCNT content remains unclear and deserves investigation.

As demonstrated in figure 6(a), a printed flat composite sample with 25 wt% MWCNTs (57 mm length, 6 mm width, and 1.6 mm thickness) was twisted by 1080 degree at 90 °C and stabilized for a given time. Then, the sample was cooled back to room temperature while maintaining force. After unloading, the sample was heated up to 90 °C again to examine the shape fixity. The shape-reforming degree strongly depends on the stabilization time at high temperatures. With a

short heating period (~1 min), the sample recovered the original shape automatically at 90 °C, showing the conventional shape memory effect of polymeric materials. With a long stabilization time (30 min), the shape was reformed without notable recovery. This happened because the internal stress during the stabilization was gradually released due to the BERs.

Parametric studies were performed to examine the influences of programming temperature and time on the shape fixity of polyimine composites. During the tests, a flat composite sample was wrapped around a cylinder aluminum mold (22 mm in diameter) at a specific programming temperature, and the deformation was held for a given time. The force applied for programming was small, only serving to maintain the deformation. The temperature was then cooled back to room temperature while maintaining force. After unloading, the sample was heated up to 90 °C again and stabilized for 5 min to examine the shape-reforming capability, which was characterized by the bending curvature (κ) of the reprocessed composite sample. A unitless shape fixity ratio is defined as $R_f = \kappa/\kappa_0$, with κ_0 being the reciprocal of the mold radius. $R_f = 1$ suggests a complete shape-reforming without shape recovery after unloading.

The shape fixity of the polyimine composites after heating for different times are summarized in figure 6(b), where the temperature is 50 °C, 60 °C, 70 °C, 80 °C, and 90 °C,
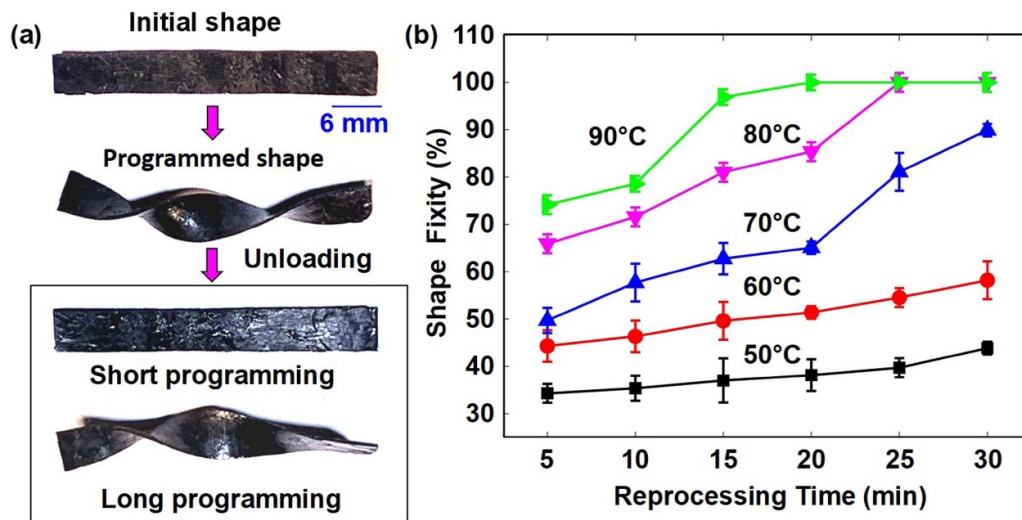
Figure 6. (a) Demonstration of the shape-reforming ability of the printed polyimine composites. (b) Shape-reforming degree of the polyimine composite as a function of stabilization time and programming temperature.

respectively. It is observed that both the temperature and heating time promote the shape fixity of the polyimine composite, because these two parameters play an equivalent role in determining the extent of BER-induced stress relaxation of the polyimine matrix. Even with considerable MWCNT content, the composites are still able to completely fix the programming shape at elevated temperatures or using an extended heating time. At 90 °C, the polyimine composites can be fully reshaped after ~15 min. It should be noted that with a higher programming curvature, the final shape fixity of the composite may be lower than 100%, because the MWCNTs would provide a higher resistance force for the shape-reforming.

2.4. Joule heat-induced self-healing of the polyimine composites

Since the printed polyimine composites are electrically conductive, they can be welded using Joule heating induced by electricity. Herein, the polyimine composite with 25 wt% MWCNTs was used as a material platform to examine the healing efficiency in terms of mechanical strength and conductivity. As shown in figure 7(a), a cylindrical sample (extruded using a syringe with 3.3 mm diameter needle) was first cut in half using a razor and then brought together using a tweezer with a small squeezing force being applied to maintain good contact. A direct current was applied through two probes at a 5 mm distance to introduce Joule heating, which triggers the BERs in the polyimine matrix and the connection of polymer chains on the interface. This will also lead to the diffusion of nanoparticles to form conductive pathways across the interface. After being heated for a given time, the two parts were joined for testing. The appearance of the polyimine composite sample during the welding is shown in figure 7(b). During the experiments, a 0.15 Amperes current was applied, and the voltage slightly decreased from 0.17 Volts due to the increase of resistance and temperature (see figure 5(a)). Using an infrared camera (FLIR Systems, Inc., Wilsonville, USA),

it was observed that the temperature around the interface increased rapidly. Due to the natural convection, the temperature eventually saturated around 63 °C after 5 min, which was sufficiently high for the interfacial welding.

The conductivity of the welded polyimine composite was determined using the four-point probe resistivity measurement. Its mechanical strength was tested using the uniaxial tension tests at room temperature on the MTS machine. The increment of the conductivity and ultimate strength of the welded sample is plotted in figure 7(c) as a function of welding time. It is observed that the conductivity reaches the same level as that of the fresh sample (2.7 s cm^{-1}) after being welded for ~40 min. The ultimate strength saturates at ~57 MPa after ~50 min of welding. But the strength value is slightly lower than that of the fresh sample (~70 MPa). This might result from the interfacial voids after the welding as the samples exhibit rough surfaces after razor cutting. The strength should be increased when using a higher welding pressure to ensure a defect-free interface.

The cutting-welding process was repeated three times in the same location as the sample. In each cycle, the sample was welded using the same current for 50 min. The final conductivity and mechanical strength of the sample in each welding cycle are summarized in figure 7(d). Despite the lower interfacial strength after welding, both two parameters were at near-identical levels after being welded three times, which suggests good repeatability of the welding process.

3. 3D printing of temperature sensors using the polyimine composites

The polyimine and conductive polyimine composites were used for the 3D printing of temperature sensors using the DIW method. The overall manufacturing process is shown in figure 8. A polyimine substrate was first printed with a dimension of 40 mm by 60 mm (figure 8(a)). The substrate exhibited a rough surface due to the nature of the DIW printing
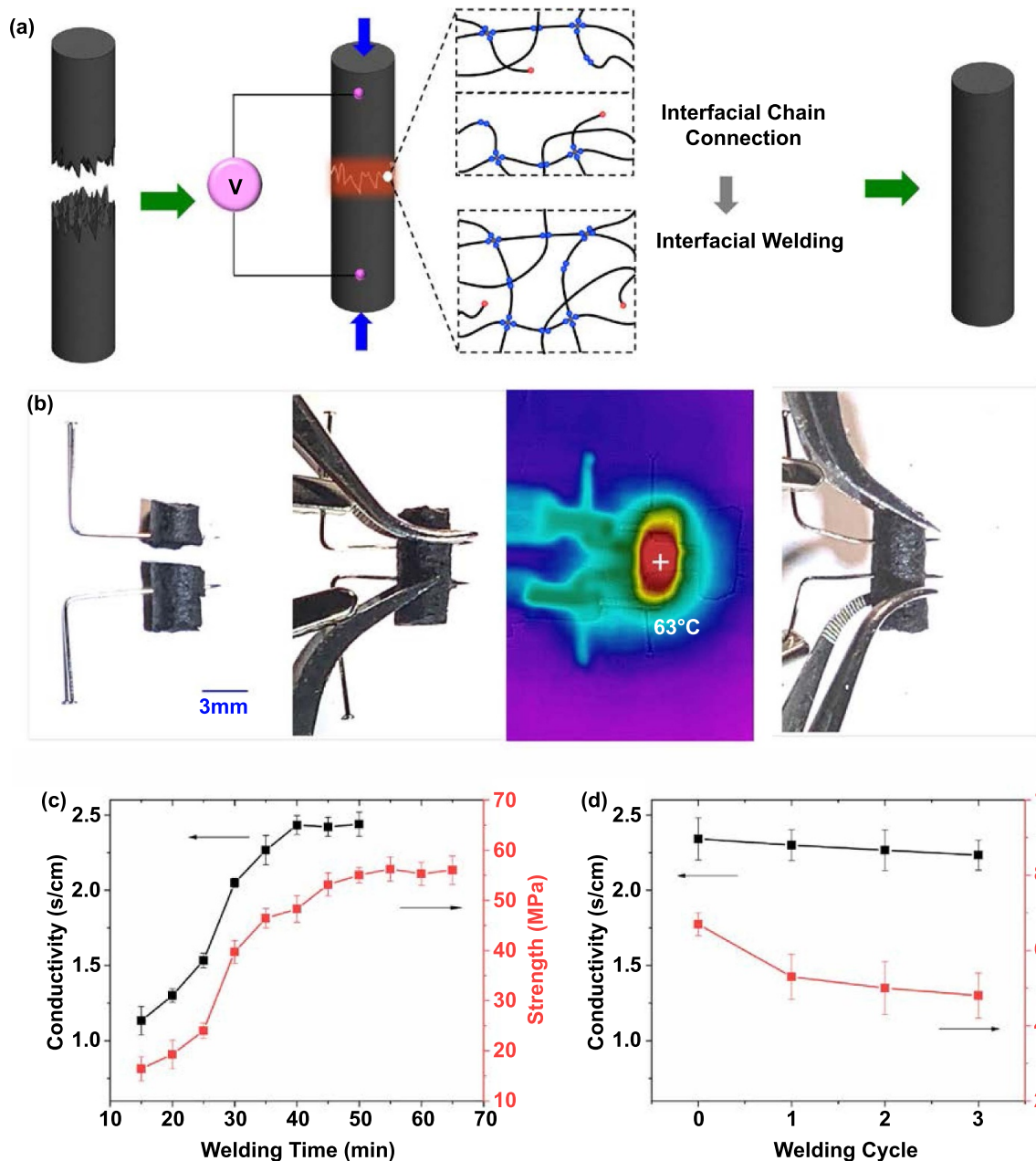
Figure 7. (a) Schematic views of the welding process of polyimine composites using Joule heat induced by electricity. (b) Appearances of the sample during the welding. (c) The increment of conductivity and mechanical strength of polyimine composite as a function of welding time. (d) The ultimate conductivity and mechanical strength of the welded polyimine composites in the first three welding cycles.

of filaments. To enable a smooth surface, the printed sample was subject to hot pressing at 90 °C with a 0.1 MPa pressure applied (figure 8(b)). This will enable a good bonding with conductive polyimine composites printed on the surface. After pressing, the sample thickness was ∼0.11 mm (figure 8(c)).

Conductive ink was then printed on the substrate surface with a defined pattern (figure 8(d)). The printout was then transferred into an oven to post-cure the conductive ink and obtain the final temperature sensor (figure 8(e)). As demonstrated in the previous sections, the sensor is malleable due to the polyimine matrix and can be reshaped into different geometries depending on the applications (figure 8(f)). It can be repaired after damage based on the interfacial welding effect

(figure 8(g)). Finally, the temperature sensor was recycled using the amine-containing solvent. They can be fully depolymerized in the propylamine solvent at 80 °C (figure 8(h)). Since the polyimine substrate was depolymerized, additional MWCNTs were added into the solution to maintain the same ratio between polyimine and MWCNTs. The polymer solution was partially cured reloaded into the DIW printer as a new ink for the next round of printing on a new polyimine substrate.

The appearance of a 3D printed sensor is show in figure 9(a), wherein the conductive polyimine contains 25 wt% MWCNTs. No notable shape distortion is observed after the post-curing of the polyimine composite. As shown in
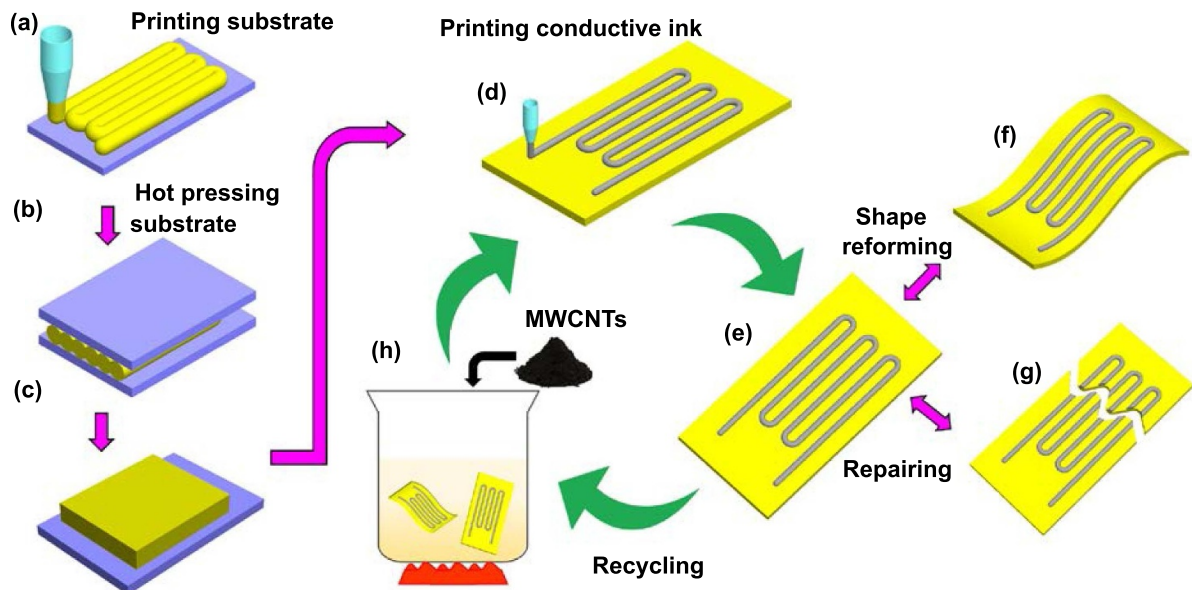
Figure 8. (a)–(h) Overall manufacturing process of the temperature sensor.
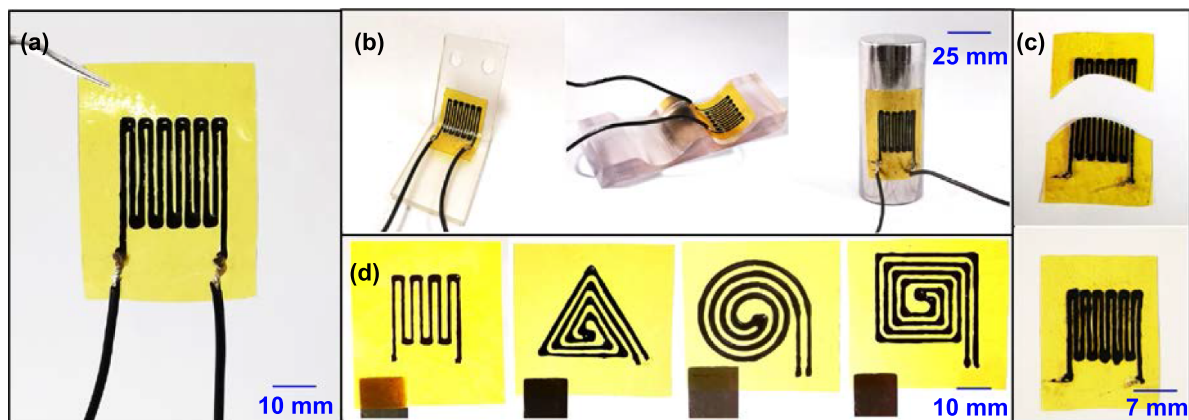
Figure 9. Photographs of 3D-printed sensor patterns. (a) The appearance of the printed temperature sensor. (b) Demonstration of the shape-reforming capability of the printed sensor. (c) The printed sensor can be repaired after damage based on the interfacial welding effect of polyimine. (d) The printed sensor can be fully repaired using amine-containing solvent. The pictures show the printed sensors with different patterns of conductive lines during the recyclable 3D printing.

figure 9(b), the malleable sensor can be easily mounted onto the surfaces of 3D components in different shapes after heating using a heat gun. The sensor also exhibits self-healing capability. As shown in figure 9(c), the printed sensor was manually cut using a razor. They were then brought together and sandwiched between two glass slides. After heating at 90 °C for 40 min with a relatively small pressure (∼0.1 MPa) applied, the sensor was repaired, and the pattern of the conductive lines are seen to be maintained. The recyclability of the printed sensor is shown in figure 9(d), wherein the printed sensor was fully decomposed in the amine-containing solvent. Equivalent amount of MWCNTs was added into the solution to make sure the MWCNT content is 25 wt% compared to the polyimine resin. After pre-curing to increase the resin viscosity, it was used to print temperature sensors with different patterns of conductive line. The ink maintained a good printability in each printing cycle.

The characterizations on the printed temperature sensor are presented in figure 10, where the temperature was increased linearly from room temperature to 60 °C at 2 °C min^{-1}. As shown in figure 5(a), the conductivity of the polyimine composite is sensitive to temperature changes. Since it decreases with temperature linearly within the tested temperature range, the sensor resistance increases with temperature and the sensitivity was measured to be ∼0.13%/°C. In addition, the repaired and recycled sensors as demonstrated in figure 9 are also characterized. They exhibit close performance to that of a newly printed sensor. The comparison in figure 10 suggests that the developed polyimine composite sensor possesses excellent repairing and recycling capabilities.

Note that the characterizations on the temperature sensor were performed in the free-standing state without applying the mechanical loading. The polyimine exhibits stable material properties at temperatures up to 150 °C. Increasing
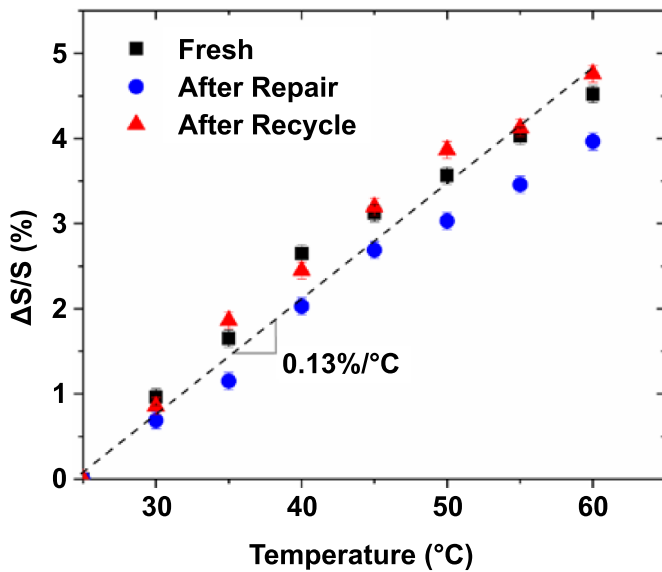
Figure 10. The characterizations on the printed temperature sensor. The performance of repaired and recycled sensor is compared to that of a newly printed one.

the temperature any further might lead to thermal degradation or notable oxidization of the polyimine matrix. However, if the sensor is applied with mechanical loading, the limit of the temperature measurement might be lower than 150 °C. At high temperatures, the polyimine matrix is malleable and experiences creep deformation due to active BERs. The temperature-conductivity relationship of the polyimine composites will change with deformation, and, thus, affect the performance of the sensor. It remains unclear to us what the upper limit of the temperature measurement is when the sensor is subject to various loading conditions. This is an important topic that deserves further study.

4. Conclusion

In summary, conductive polyimine composites were used to fabricate polymeric electronics using the DIW 3D printing method. The adopted materials enabled the reshapeability, repairability, and recyclability of printed electronics. A conductive polyimine ink containing MWCNTs was first developed. It was found that the ink containing 10 wt% nanoclay and 25 wt% MWCNTs exhibited high yielding strength, a notable shear-thinning effect, and good conductivity ($\sim$2.7 s cm^{-1}), which is suitable for the DIW 3D printing. The ink was fully recyclable for repeated 3D printing of polyimine composites. Due to the covalent bonding among filaments, the printed polyimine composites exhibited near-identical mechanical properties and conductivity in different directions. The composites' conductivity first decreased with the temperature due to the disruption of conductive pathways by BERs, and then started to increase after the pathways were reorganized. The conductivity also changed linearly with different tensile and compressive strains. The shape-reforming capability of conductive polyimine composites was

investigated with different programming temperatures and times. It shows that even with a considerable amount of MWCNT in the matrix, the polyimine can completely fix the programming shape using a high temperature or an extended heating time. The printed polyimine composites also demonstrated robust interfacial welding capability by using the Joule heating induced by electricity. During the repeated welding-cutting process at the same location, the samples maintained almost the same level of conductivity. The mechanical strength was slightly low but could be improved using a higher welding pressure. Finally, a temperature sensor was printed and characterized. It was easily mounted onto the 3D surfaces, repaired after damage, and recycled using the solvent. The sensing capability of printed sensors was maintained after the repairing and recycling. Our study opens new possibilities for the development of CAN-based conductive composites for novel 3D printable reshapeable, rehealable and fully recyclable electronics targeting a broad range of sustainable applications.

5. Experimental section

5.1. Measurements on the ink rheological properties

The apparent viscosity and shear storage modulus of the prepared polyimine inks were characterized at room temperature using a rheometer (TA Instruments, AR-G2, New Castle, DE, USA). The rheometer was equipped with parallel plates with a diameter of 20 mm diameter. To test the ink viscosity, the resin was filled in the 1 mm gap between the two plates. The shear rate changed between 10^{-3} and 200 s^{-1}. To determine the modulus, the parallel plates oscillated at 1 Hz, and the stress level ranged between 0.01 Pa and 10^4 Pa.

5.2. DIW 3D printing

The 3D printing was performed using a customized DIW printer. The printable ink was loaded in a plastic syringe with a deposition nozzle (1.63 mm diameter). The syringe was connected to a digital pump (Ultimus V high precision dispenser, electron fusion devices (EFD)) to control the deposition pressure at 80 psi. A Makebot moving stage was used to control the motion of the deposition syringe.

After the polyimine composites were printed, they were moved into a vacuum oven for post-curing. The temperature was first set to be 45 °C with an 8 kPa vacuum pressure. After the printed composites gaining sufficient stiffness, the temperature was further increased to 80 °C, and the printouts were fully cured after $\sim$6 h.

To recycle the printed polyimine and their composites, they were immersed in the amine solvent. After they were fully depolymerized, the polymer solution was partially cured and loaded into the DIW printer for the next round of printing.

5.3. Measurements on the resistance of printed polyimine composites

The printed conductive polyimine composites with different MWCNT contents were cut into the same dimension of

1.6 mm × 10 mm × 40 mm. The four-point probe method was used in this study, and each data were calculated by taking the average value of six readings from six different pieces of the same specimen. The voltage between two probes was measured by a digital multimeter, and the corresponding electric resistivity was calculated according to the specimen dimension.

The specimen conductivity was measured at different temperatures. During the tests, the specimen was connected to the multimeter to read resistance change in real-time. The temperature was increased from 25 °C to 145 °C at 2 °C min^{-1}. The specimen conductivity was also measured with different tensile and compressive strain levels. The tests were performed on an MTS tester (Insight 30, New Eden Prairie, MN). Specifically, cylindrical samples with a dimension of 9.3 mm (diameter) × 14.3 mm (height) were fabricated. During the tests, the specimens were respectively stretched or compressed up 10% engineering strain at 2%/min, with the conductivity being measured in real-time using the four-point probe method.

5.4. Measurements on the mechanical properties of printed polyimine composites

The mechanical properties of the printed polyimine composites, as well as the composites after welding using Joule heating, were tested using the uniaxial tension test at room temperature. The tests were performed on an MTS tester (Insight 30, New Eden Prairie, MN). For the printed polyimine composites, the sample dimension is 1.6 mm × 10 mm × 75 mm, for the welded polyimine composites, the dimension of the cylindrical sample is 3.3 mm (diameter) × 25 mm (height). The specimen was stretched on the Bose electro-force tester, and the strain rate was set to be 5%/min for all cases.

Acknowledgments

ORCID iD

Kai Yu ⬤ https://orcid.org/0000-0001-9067-1673

References

[1] Cui J R and Forssberg E 2003 Mechanical recycling of waste electric and electronic equipment: a review *J. Hazard. Mater.* **99** 243–63

[2] Cui J R and Zhang L F 2008 Metallurgical recovery of metals from electronic waste: a review *J. Hazard. Mater.* **158** 228–56

[3] Wong M H, Wu S C, Deng W J, Yu X Z, Luo Q, Leung A O W, Wong C S C, Luksemburg W J and Wong A S 2007 Export of toxic chemicals—a review of the case of uncontrolled electronic-waste recycling *Environ. Pollut.* **149** 131–40

[4] Scott T F, Schneider A D, Cook W D and Bowman C N 2005 Photoinduced plasticity in cross-linked polymers *Science* **308** 1615–7

[5] Scott T F, Draughon R B and Bowman C N 2006 Actuation in crosslinked polymers via photoinduced stress relaxation *Adv. Mater.* **18** 2128–32

[6] Montarnal D, Capelot M, Tournilhac F and Leibler L 2011 Silica-like malleable materials from permanent organic networks *Science* **334** 965–8

[7] Capelot M, Montarnal D, Tournilhac F and Leibler L 2012 Metal-catalyzed transesterification for healing and assembling of thermosets *J. Am. Chem. Soc.* **134** 7664–7

[8] Jin Y, Yu C, Denman R J and Zhang W 2013 Recent advances in dynamic covalent chemistry *Chem. Soc. Rev.* **42** 6634–54

[9] Taynton P, Yu K, Shoemaker R K, Jin Y H, Qi H J and Zhang W 2014 Heat- or water-driven malleability in a highly recyclable covalent network polymer *Adv. Mater.* **26** 3938–42

[10] Ponnuswamy N, Cougnon F B L, Clough J M, Pantos G D and Sanders J K M 2012 Discovery of an organic trefoil knot *Science* **338** 783–5

[11] Li J, Carnall J M A, Stuart M C A and Otto S 2011 Hydrogel formation upon photoinduced covalent capture of macrocycle stacks from dynamic combinatorial libraries *Angew. Chem., Int. Ed.* **50** 8384–6

[12] Jin Y, Lei Z, Taynton P, Huang S and Zhang W 2019 Malleable and recyclable thermosets: the next generation of plastics *Matter* **1** 1456–93

[13] Zhang Y, Broekhuis A A and Picchioni F 2009 Thermally self-healing polymeric materials: the next step to recycling thermoset polymers? *Macromolecules* **42** 1906–12

[14] Chen X, Wudl F, Mal A K, Shen H and Nutt S R 2003 New thermally remendable highly cross-linked polymeric materials *Macromolecules* **36** 1802–7

[15] Chen X X, Dam M A, Ono K, Mal A, Shen H B, Nutt S R, Sheran K and Wudl F 2002 A thermally re-mendable cross-linked polymeric material *Science* **295** 1698–702

[16] Yu K, Taynton P, Zhang W, Dunn M L and Qi H J 2014 Reprocessing and recycling of thermosetting polymers based on bond exchange reactions *RSC Adv.* **4** 10108–17

[17] Yu K, Shi Q, Li H, Jabour J, Yang H, Dunn M L, Wang T and Qi H J 2016 Interfacial welding of dynamic covalent network polymers *J. Mech. Phys. Solids* **94** 1–17

[18] Yu K, Shi Q, Wang T, Dunn M L and Qi H J 2016 A computational model for surface welding in covalent adaptable networks using finite element analysis *J. Appl. Mech.* **83** 091002

[19] Yu K, Taynton P, Zhang W, Dunn M L and Qi H J 2014 Influence of stoichiometry on the glass transition and bond exchange reactions in epoxy thermoset polymers *RSC Adv.* **4** 48682–90

[20] He X, Hanzon D W and Yu K 2018 Cyclic welding behavior of covalent adaptable network polymers *J. Polym. Sci.* B **56** 402–13

[21] Johnson L M, Ledet E, Huffman N D, Swarner S L, Shepherd S D, Durham P G and Rothrock G D 2015 Controlled degradation of disulfide-based epoxy thermosets for extreme environments *Polymer* **64** 84–92

[22] de Luzuriaga A R, Martin R, Markaide N, Rekondo A, Cabañero G, Rodríguez J and Odriozola I 2016 Epoxy resin with exchangeable disulfide crosslinks to obtain reprocessable, repairable and recyclable fiber-reinforced thermoset composites *Mater. Horiz.* **3** 241–7

[23] Shi Q, Yu K, Dunn M L, Wang T J and Qi H J 2016 Solvent assisted pressure-free surface welding and reprocessing of malleable epoxy polymers *Macromolecules* **49** 5527–37

[24] He X, Lei Z, Zhang W and Yu K 2018 Recyclable 3d printing of polyimine-based covalent adaptable network polymers *3D Print. Addit. Manuf.* **5** 29–35

[25] Wang C, Goldman T M, Worrell B T, McBride M K, Alim M D and Bowman C N 2018 Recyclable and repolymerizable thiol–X photopolymers *Mater. Horiz.* **5** 1042–6

[26] Taynton P, Ni H G, Zhu C P, Yu K, Loob S, Jin Y H, Qi H J and Zhang W 2016 Repairable woven carbon fiber composites with full recyclability enabled by malleable polyimine networks *Adv. Mater.* **28** 2904–9

[27] Shi X, Luo C, Lu H and Yu. K 2019 Primary recycling of anhydride-cured engineering epoxy using alcohol solvent *Polym. Eng. Sci.* **59** E111–9

[28] Yu K, Yang H, Dao B H, Shi Q and Yakacki C M 2017 Dissolution of covalent adaptable network polymers in organic solvent *J. Mech. Phys. Solids* **109** 78–94

[29] Shi X, Soule D, Mao Y, Yakacki C, Lu H and Yu. K 2020 A multiscale chemomechanics theory for the solvent–assisted recycling of covalent adaptable network polymers *J. Mech. Phys. Solids* **138** 103918

[30] He X, Ding Y, Lei Z, Welch S, Zhang W, Dunn M and Yu K 2021 3d printing of continuous fiber-reinforced thermoset composites *Addit. Manuf.* **40** 101921

[31] He X, Shi X, Chung C, Lei Z, Zhang W and Kai Y 2021 A sustainable manufacturing method of thermoset composites based on covalent adaptable network polymers *Composites* B **221** 109004

[32] Kai Y, Shi Q, Dunn M L, Wang T and Qi H J 2016 Carbon fiber reinforced thermoset composite with near 100% recyclability *Adv. Funct. Mater.* **26** 6098–106

[33] Li Y, Chen S S, Wu M C and Sun J Q 2012 Polyelectrolyte multilayers impart healability to highly electrically conductive films *Adv. Mater.* **24** 4578–82

[34] Williams K A, Boydston A J and Bielawski C W 2007 Towards electrically conductive, self-healing materials *J. R. Soc. Interface* **4** 359–62

[35] Hou C Y, Huang T, Wang H Z, Yu H, Zhang Q H and Li Y G 2013 A strong and stretchable self-healing film with self-activated pressure sensitivity for potential artificial skin applications *Sci. Rep.* **3** 3138

[36] Tee B C K, Wang C, Allen R and Bao Z N 2012 An electrically and mechanically self-healing composite with pressure- and flexion-sensitive properties for electronic Skin Applications *Nat. Nanotechnol.* **7** 825–32

[37] Zou Z N, Zhu C P, Li Y, Lei X F, Zhang W and Xiao J L 2018 Rehealable, fully recyclable, and malleable electronic skin enabled by dynamic covalent thermoset nanocomposite *Sci. Adv.* **4** eaaq0508

[38] Shi C, Zou Z, Lei Z, Zhu P, Zhang W and Xiao J 2020 Heterogeneous integration of rigid, soft, and liquid materials for self-healable, recyclable, and reconfigurable wearable electronics *Sci. Adv.* **6** eabd0202

[39] Wang C, Wu H, Chen Z, McDowell M T, Cui Y and Bao Z A 2013 Self-healing chemistry enables the stable operation of silicon microparticle anodes for high-energy lithium-ion batteries *Nat. Chem.* **5** 1042–8

[40] Blaiszik B J, Kramer S L B, Grady M E, McIlroy D A, Moore J S, Sottos N R and White S R 2012 Autonomic restoration of electrical conductivity *Adv. Mater.* **24** 398

[41] Odom S A, Chayanupatkul S, Blaiszik B J, Zhao O, Jackson A C, Braun P V, Sottos N R, White S R and Moore J S 2012 A self-healing conductive ink *Adv. Mater.* **24** 2578–81

[42] Toohey K S, Sottos N R, Lewis J A, Moore J S and White S R 2007 Self-healing materials with microvascular networks *Nat. Mater.* **6** 581–5

[43] Odom S A, Caruso M M, Finke A D, Prokup A M, Ritchey J A, Leonard J H, White S R, Sottos N R and Moore J S 2010 Restoration of conductivity with Ttf-Tcnq charge-transfer salts *Adv. Funct. Mater.* **20** 1721–7

[44] Berman B 2012 3D printing: the new industrial revolution *Bus. Horiz.* **55** 155–62

[45] Ngo T D, Alireza K, Gabriele I, Kate T N and Hui D 2018 Additive manufacturing (3d printing): a review of materials, methods, applications and challenges *Compos. B Eng.* **143** 172–96

[46] Gebler M, Uiterkamp A J M S and Visser C 2014 A global sustainability perspective on 3d printing technologies *Energy Policy* **74** 158–67

[47] Pengcheng W, Wang Z, Yao X, Jianzhong F and Yong H 2021 Recyclable conductive nanoclay for direct *in situ* printing flexible electronics *Mater. Horiz.* **8** 2006–17

[48] Wu P, Zhou L, Lv S, Fu J and He. Y 2021 Self-sintering liquid metal ink with laponite® for flexible electRONICS *J. Mater. Chem.* C **9** 3070–80

[49] Kumar D and Sharma R C 1998 Advances in conductive polymers *Eur. Polym. J.* **34** 1053–60

[50] Tseghai G B, Mengistie D A, Malengier B, Fante K A and Van Langenhove L 2020 Pedot: pss-based conductive textiles and their applications *Sensors* **20** 1881

[51] Wang Y, Liu A, Han Y and Li T 2020 Sensors based on conductive polymers and their composites: a review *Polym. Int.* **69** 7–17

[52] Cho J W, Kim J W, Jung Y C and Goo N S 2005 Electroactive shape-memory polyurethane composites incorporating carbon nanotubes *Macromol. Rapid Commun.* **26** 412–6

[53] Coleman J N, Khan U, Blau W J and Gun'ko Y K 2006 Small but strong: a review of the mechanical properties of carbon nanotube-polymer composites *Carbon* **44** 1624–52

[54] Guo W H, Liu C, Sun X M, Yang Z B, Kia H G and Peng H S 2012 Aligned carbon nanotube/polymer composite fibers with improved mechanical strength and electrical conductivity *J. Mater. Chem.* **22** 903–8

[55] Chae J Y, Yoo H J, Kim Y A, Cho J W and Endo M 2010 Electroactive shape memory performance of polyurethane composite having homogeneously dispersed and covalently crosslinked carbon nanotubes *Carbon* **48** 1598–603

[56] Koerner H, Price G, Pearce N A, Alexander M and Vaia R A 2004 Remotely actuated polymer nanocomposites—stress-recovery of carbon-nanotube-filled thermoplastic elastomers *Nat. Mater.* **3** 115–20

[57] Yu K, Liu Y and Leng J 2011 Conductive shape memory polymer composite incorporated with hybrid fillers: electrical, mechanical, and shape memory properties *J. Intell. Mater. Syst. Struct.* **22** 369–79

[58] Yu K, Liu Y, Liu Y, Peng H-X and Leng J 2013 Mechanical and shape recovery properties of shape memory polymer composite embedded with cup-stacked carbon nanotubes *J. Intell. Mater. Syst. Struct.* **25** 1264–75

[59] Yu K, Zhang Z, Liu Y and Leng J 2011 Carbon nanotube chains in a shape memory polymer/carbon black composite: to significantly reduce the electrical resistivity *Appl. Phys. Lett.* **98** 074102

[60] Lewis J A 2006 Direct ink writing of 3d functional materials *Adv. Funct. Mater.* **16** 2193–204

[61] Lewis J A and Gratson G M 2004 Direct writing in three dimensions *Mater. Today* **7** 32–39

[62] Gratson G M, Xu M J and Lewis J A 2004 Microperiodic structures—direct writing of three-dimensional webs *Nature* **428** 386

[63] Adams J J, Duoss E B, Malkowski T F, Motala M J, Ahn B Y, Nuzzo R G, Bernhard J T and Lewis J A 2011 Conformal printing of electrically small antennas on three-dimensional surfaces *Adv. Mater.* **23** 1335–40

[64] Wei M, Zhang F, Wang W, Alexandridis P, Zhou C and Wu G 2017 3d direct writing fabrication of electrodes for electrochemical storage devices *J. Power Sources* **354** 134–47

[65] Fu K *et al* 2016 Graphene oxide-based electrode inks for 3d-printed lithium-ion batteries *Adv. Mater.* **28** 2587

[66] Milroy C and Manthiram A 2016 Printed microelectrodes for scalable, high-areal-capacity lithium-sulfur batteries *Chem. Commun.* **52** 4282–5

[67] Ho C C, Evans J W and Wright P K 2010 Direct write dispenser printing of a zinc microbattery with an ionic liquid gel electrolyte *J. Micromech. Microeng.* **20** 104009

[68] Sun K, Wei T S, Ahn B Y, Seo J Y, Dillon S J and Lewis J A 2013 3d printing of interdigitated li-ion microbattery architectures *Adv. Mater.* **25** 4539–43

[69] Kong Y L, Tamargo I A, Kim H, Johnson B N, Gupta M K, Koh T W, Chin H A, Steingart D A, Rand B P and McAlpine M C 2014 3d printed quantum dot light-emitting diodes *Nano Lett.* **14** 7017–23

[70] Valentine A D, Busbee T A, Boley J W, Raney J R, Chortos A, Kotikian A, Berrigan J D, Durstock M F and Lewis J A 2017 Hybrid 3d printing of soft electronics *Adv. Mater.* **29** 1703817

[71] Guo S Z, Qiu K Y, Meng F B, Park S H and McAlpine M C 2017 3d printed stretchable tactile sensors *Adv. Mater.* **29** 1701218

[72] Es-Said O S, Foyos J, Noorani R, Mendelson M, Marloth R and Pregger B A 2000 Effect of layer orientation on mechanical properties of rapid prototyped samples *Mater. Manuf. Process.* **15** 107–22

[73] Cunha M A G and Robbins M O 2020 Effect of flow-induced molecular alignment on welding and strength of polymer interfaces *Macromolecules* **53** 8417–27

[74] Tosto C, Saitta L, Pergolizzi E, Blanco I, Celano G and Cicala G 2020 Methods for the characterization of polyetherimide based materials processed by fused deposition modelling *Appl. Sci.* **10** 3195

[75] Nor Ashikin N F, Shuib R K, Ku Ishak K M, Hamid Z A A, Abdullah M K and Rusli A 2021 Thermal and rheological properties of self-fabricated polyethylene glycol-plasticized poly (lactic acid) filaments for fused deposition modeling *Prog. Rubber Plast. Recycl. Technol.* **37** 19–31

[76] Zhang J, Lei Z, Luo S, Jin Y, Qiu L and Zhang W 2020 Malleable and recyclable conductive mwcnt-vitrimer composite for flexible electronics *ACS Appl. Nano Mater.* **3** 4845–50

[77] Stauffer D and Aharony A 1994 *Introduction to Percolation Theory* (London, UK: Taylor & Francis)

[78] Shi X, Ge Q, Lu H and Yu. K 2021 The nonequilibrium behaviors of covalent adaptable network polymers during the topology transition *Soft Matter* **17** 2104–19

[79] Wang T X, Chen H M, Salvekar A V, Lim J, Chen Y, Xiao R and Huang W M 2020 Vitrimer-like shape memory polymers: characterization and applications in reshaping and manufacturing *Polymers* **12** 2330